Supplemental Material for "Neural Network Approach for Characterizing Structural Transformations by X-ray Absorption Fine Structure Spectroscopy"

Janis Timoshenko,[1] Andris Anspoks,[2] Arturs Cintins,[2] Alexei Kuzmin,[2] Juris Purans,[2] and Anatoly I. Frenkel[1,3]

[1]*Department of Materials Science and Chemical Engineering, Stony Brook University, Stony Brook, NY 11794, USA**

[2]*Institute of Solid State Physics, University of Latvia, Kengaraga Street 8, Riga, LV-1063, Latvia*

[3]*Division of Chemistry, Brookhaven National Laboratory, Upton, NY 11973, USA*†

I. DETAILS OF NEURAL NETWORK IMPLEMENTATION AND TRAINING

Artificial neural network (NN) was constructed and its training was performed using the off-the-shelf available NN implementation in *Wolfram Mathematica* 11.2 [1]. Schematically the used NN is depicted in Fig. 1 in the main text. It consists of (i) an input layer with ca 600 nodes, initialized with experimental or theoretical EXAFS data, mapped by Morlet wavelet transformation (WT) [2, 3] to (k, R)-space, (ii) two hidden layers with ca 600 nodes in each, and (iii) the output layer with 100 nodes, where the output values for different nodes correspond to a specific bin height in a histogram that parameterizes the radial distribution function (RDF) in the R-range between 2.0 Å and 6.0 Å. Bin width is 0.04 Å.

As explained in the main text, each node in the NN performs a simple operation: all its inputs $x^{[n-1](i)}$ are weighted with some weights $\theta^{[n](i,j)}$ and added together (unit feature $x^{[n-1](0)} = 1$ is appended to the input to account for bias term). Some non-linear, differentiable function (so called activation function) f is then applied to the sum, and the output $x^{[n](j)} = f(\sum x^{[i-1](i)}\theta^{[n](i,j)})$ can then be similarly processed in the nodes in the consequent NN layers. As activation function for hidden layers we use hyperbolic tangent function, while linear function is used for the output nodes.

The use of WT for NN input is beneficial, since sensitivity of WT to features in R-space ensures the spatial resolution of our method, while its sensitivity to features in k-space allows us to probe the dampening of EXAFS oscillations, which is directly related to the disorder, and for multielement systems ensures chemical sensitivity [2, 4]. We do not use all WT points for the NN analysis, but only those that are most sensitive to changes in structure. The corresponding region in (k, R)-space is identified automatically based on the analysis of the spectra in the training data set: for each of the spectra χ_t in the training data set we calculate the corresponding WT, and calculate the variance of the obtained WT values at different k and R points. Only the region, where the variance is larger than 5% of the maximal observed variance value, is used for further analysis. The non-trivial shape of this region is shown in Fig. 1(c) in the main text. Such filtering allows us to stabilize the procedure by excluding the points that do not contain useful structural information but may be affected by systematic errors, e.g., by the artifacts of the procedure, used to extract EXAFS signals from the experimentally measured total X-ray absorption spectra, or by inaccuracies of EXAFS simulations in theoretically modeled spectra (used for NN training). Note also that the Morlet WT [2, 3], which is employed here, is a complex transformation, and, in principle, one can use both imaginary and real parts of WT to initialize NN input layer. In practice, however, we have found that better performance can be ensured, if as input for NN we use WT absolute value.

To generate training data set, we rely on classical molecular dynamics (MD) simulations, followed by calculations of corresponding theoretical EXAFS spectra. Similarly as in our previous works [4, 5] for MD simulations we employ Sutton-Chen force field model [6], with the values for empirical parameters taken from [7].

MD simulations are performed with GULP code [8, 9] in the canonical ensemble. We use periodic boundary conditions. Simulation box has a size of the $5a_0 \times 5a_0 \times 5a_0$ supercell for body-centered cubic (BCC) structure of iron including thus 250 atoms, and $4a_0 \times 4a_0 \times 4a_0$ supercell for face-centered cubic (FCC) structure including thus 256 atoms (there are two and four atoms, respectively, in the unit cell of BCC and FCC structures). The temperature-dependent lattice constants a_0 used for MD simulations are taken from XRD results [10], and extrapolated for the temperatures, where experimental data are not available. For completeness, we performed also MD simulations for iron with hexagonal close-packed (HCP) structure with $8a_0 \times 4a_0 \times 4c_0$ supercell (256 atoms). For simulations at all temperatures for HCP structure we used $a_0 = 2.507$ Å, $c_0 = 4.070$ Å that correspond to the lattice constants for bulk cobalt at room temperature [11].

Note also that the crystallographic structure (BCC, FCC or HCP) in our MD models is completely defined by the initial structure model and does not change during the simulations, since the system volume is fixed within canonical

(NVT) ensemble, while the phase transition from BCC to close-packed FCC structure is associated with a significant volume reduction. Note also that even without this constraint MD simulations of this phase transition for bulk material are challenging and, typically, cannot be reproduced with such simple potentials as used here [12]. While it may seem as a limitation of MD simulations, for our purposes it is actually a benefit, since we can generate theoretical spectra corresponding to FCC, HCP and BCC phases at any temperature. For each phase MD simulations were performed in the temperature range between $T_{\min} = 10$ K and $T_{\max} = 1500$ K with the increment $\Delta T = 10$ K. $T_{\max}$ value was chosen so that it exceeds significantly the largest temperature, at which it was possible to collect the experimental data. Further reduction of ΔT value did not improve the accuracy of the trained NN. Nosé-Hoover thermostat [13] was employed to ensure the required average temperature during each MD simulation. The Newton's equations of motion were integrated using the Verlet leapfrog algorithm [14] with a time step of 0.5 fs. The equilibration time is 20 ps, followed by 20 ps of production run, during which 4000 atomic configurations are accumulated. Note also that MD models at very low temperatures (near 0 K) do not reproduce the behavior of real material, since the contribution of quantum effects in neglected.

To obtain theoretical EXAFS spectra shown in Fig. 2 in the main text, for each of the 4000 configurations, generated in MD simulations, a theoretical EXAFS averaged over all absorbing atoms is calculated using FEFF8.5L [15] software, taking into account single scattering, double scattering and triple scattering paths with half lengths up to 6.5 Å. Calculated configuration-averaged EXAFS spectra are then averaged over time, to obtain the final time- and configuration-averaged spectrum (MD-EXAFS) [5]. To generate spectra used for NN training a less accurate, but computationally more efficient procedure was used: we did not perform time-averaging in this case, only the averaging over all absorbing atoms in a single MD "snapshot" (with 250 or 256 atoms). For the low temperatures such simplification does not affect the calculated spectra, but for the higher temperatures, where correct sampling of thermal disorder is important, the deviations between ensemble-averaged and time- and ensemble-averaged spectra are noticeable.

To account for possible deviations of interatomic distances from those, defined by XRD data, we could, in principle, repeat MD simulations with different lattice parameters (since the lattice constants are just another empirical parameter in our classical MD simulations). To minimize the required computational resources, however, we simply rescaled all atomic coordinates in the obtained MD models, by changing thus all interatomic distances. For each temperature point additional 11 such rescaled models with lattice constants rescaled in the range between $\alpha_{\min} = 97\%$ and $\alpha_{\max} = 103\%$ (with the increment $\Delta\alpha = 0.6\%$) of the original one were constructed, and for each of them the corresponding EXAFS spectrum was calculated. The $\alpha_{\min}$ and $\alpha_{\max}$ values were chosen so that the variation in lattice constants in our models exceeds the thermal expansion of bulk iron [10], as well as allow us to account for the differences in lattice parameters for iron, nickel and cobalt. Inclusion of additional training models to our data set by further reducing $\Delta\alpha$ did not improve the NN accuracy.

About 3000 MD-EXAFS spectra $\chi_t(k)$ corresponding to different iron structures, temperatures and interatomic distances were obtained. As explained above, the input vectors in the training data set each contains ca 600 elements (corresponding to the values of WT at different $k-$ and R-values), but strong correlations exist between different elements of an input vector, reducing significantly the actual dimensionality of the input space. To estimate the maximal amount of information in the input spectra, we can use principal component (PC) analysis [16]. Model spectra in the training data set were used to identify the most important linearly independent PCs. The obtained PCs then can be used as basis vectors to reconstruct the original spectra. As shown in Fig. S1, 20 - 30 components are required to reconstruct the spectra in our training data set with the accuracy comparable to the noise in our experimental measurements. Next, since the corresponding true RDFs $g_t(R)$ are known for the model spectra in the training data set, we can use them to optimize the values of NN weights $\theta^{[n](i,j)}$, so that the difference between RDFs $\tilde{g}_t(R)$, predicted by NN, and the true RDFs $g_t(R)$ is minimized for all spectra in the training data set.

A small subset of generated MD-EXAFS spectra (120 spectra) was not used for NN training, but was used to validate the accuracy of the trained NN (see Fig. S2). This validation data set was used to find the optimal values for NN hyperparameters: number of hidden nodes and layers, types of activation functions, number of iterations for training, etc. were optimized so that the NN yields optimal performance on the validation data set. All hyperparameters were obtained by manual grid search (i.e., by manually trying out different combinations of hyperparameters). The best performance was achieved with the following parameters: hyperbolic tangent functions were used as activation functions (rectified linear units (RELU) were also tried out); "Adam" training algorithm (stochastic gradient descent using an adaptive learning rate) was used for NN training with default parameters values $\beta_1 = 0.9$ and $\beta_2 = 0.999$; batch size was 512; NN training was performed for 4800 training rounds. Loss function was defined as the L2-norm between output and target vectors averaged across the batch. No normalization of input or output features was used. Note that the great benefit of using such high-level programming language as *Wolfram Mathematica* is that quite complex operations, such as NN construction and optimization, can be done easily: it takes just two lines of code to

generate NN and to train it by using *NetChain* and *NetTrain* commands.

NN method provides a convenient way to estimate the uncertainties of the analysis. For this purpose we rely on so called bootstrapping method: we construct and train several (ten in our case) independent NNs. Each NN is trained only on a randomly chosen subset (80 %) of all training examples. Afterwards, as a final result we report the $\tilde{g}_t(R)$, averaged over predictions of all ten NNs, and the standard deviation of their predictions we report as the uncertainty.

To quantify the disagreement between NN prediction and true RDF, one can use the integrated squared difference $\|g(R)-\tilde{g}(R)\|^2 = \sum_i (g(R_i)-\tilde{g}(R_i))^2 \Delta R$, where ΔR is histogram bin size. For different examples in the training data set the obtained $\|g(R)-\tilde{g}(R)\|^2$ values are distributed according to an asymmetric monomodal distribution with the median at 29 Å^{-1} and the first and the last decile at 19 and 53 Å^{-1}, respectively. For the validation data set (Fig. S2), the distribution median is at 38 Å^{-1}, while the first and the last deciles - at 23 and 213 Å^{-1}. Since for experimental data (Fig. S4) we do not know the true RDFs $g(R_i)$, to quantify the accuracy of NN predictions we can use instead the result of reverse Monte Carlo (RMC) simulations. In this case the integrated squared differences between the NN prediction and RDF from RMC simulations for iron at different temperatures are in the range between 29 ± 9 Å^{-1} and 138 ± 29 Å^{-1}. For nickel and cobalt the integrated error for the averaged RDF is larger, around ca 500 Å^{-1}, and fluctuates significantly, when the results, obtained by independently trained NNs, are compared.

II. SUPPLEMENTAL FIGURES

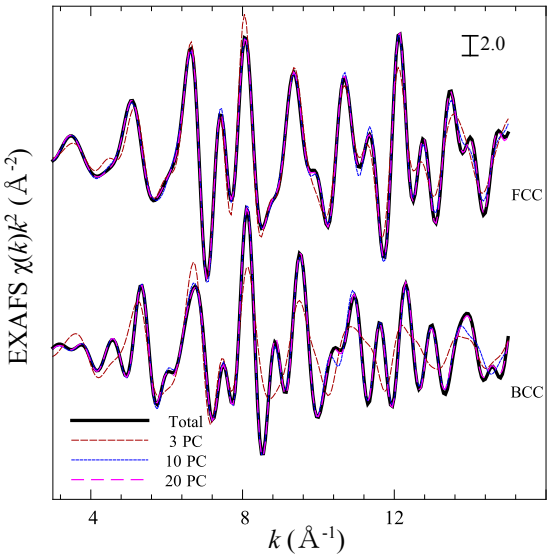

SUPPLEMENTAL FIG. 1. Estimation of the number of independent data points in the training data set using principal components (PC) analysis. Model spectra in the training data set were used to identify the most important PCs. Low-temperature (10 K) MD-EXAFS spectra for BCC and FCC iron are shown, and compared with the results of reconstruction with 3, 10 and 20 PCs.

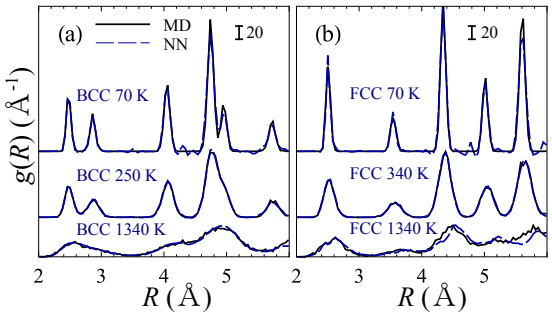

SUPPLEMENTAL FIG. 2. Validation of NN method with theoretical data (not used for NN training). RDFs $\tilde{g}(R)$ (shifted vertically for clarity) for iron, extracted by NN from theoretical EXAFS data that were calculated in MD simulations with BCC and FCC structures at different temperatures, are compared with the true values of RDFs $g(R)$, calculated directly from MD coordinates, demonstrating high accuracy of the trained NN predictions in a broad range of temperatures and both for body-centered cubic (BCC) and face-centered cubic (FCC) structures.

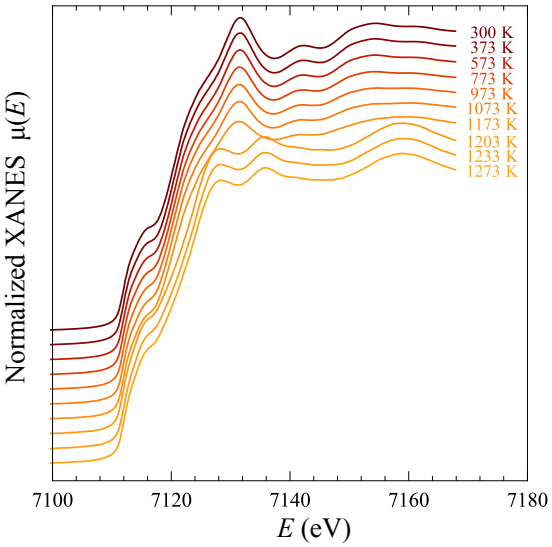

SUPPLEMENTAL FIG. 3. Experimental Fe K-edge XANES data for temperatures between 300 K and 1273 K, shifted vertically for clarity. Spectra show no changes in the sample oxidation state and structure, except the one that can be associated with the transition from ferrite to austenite at temperatures between 1173 and 1203 K. Note that the high sensitivity of Fe K-edge XANES features to structure details was demonstrated, e.g., in Ref. [17].

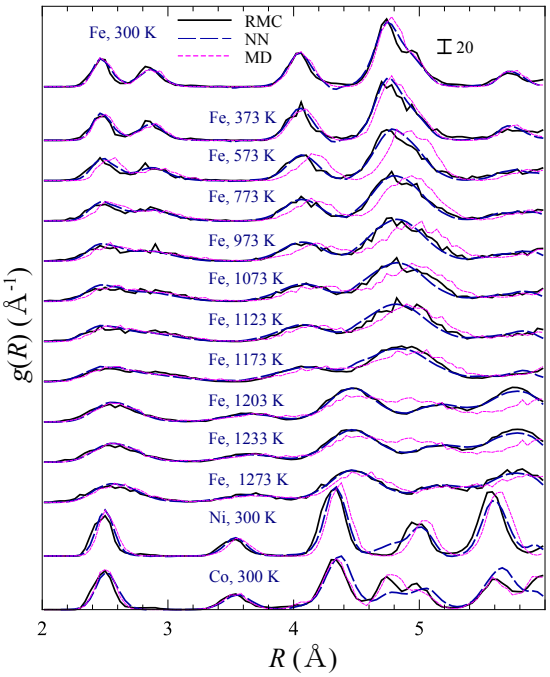

SUPPLEMENTAL FIG. 4. RDFs for bulk iron at different temperatures and bulk nickel and bulk cobalt at room temperature, obtained by NN from experimental EXAFS data (shifted vertically for clarity). For comparison the results of reverse Monte Carlo (RMC) simulations [3, 5] are also shown, as well as the results of the trivial MD spectra matching approach, where instead of being used for NN training, MD-generated EXAFS data are compared directly with experimental data, and the RDF for the model that gives the best agreement with experiment is then claimed to be the true RDF in experimental sample. Results obtained by NN are in an excellent agreement with RMC results, while the spectra matching approach fails to yield accurate RDFs for high temperatures.

* janis.timosenko@stonybrook.edu
† anatoly.frenkel@stonybrook.edu

[1] Wolfram Research Inc., *Mathematica, Version 11.2*, Champaign, IL, 2017.
[2] J. Timoshenko and A. Kuzmin, Comp. Phys. Commun. **180**, 920 (2009).
[3] J. Timoshenko, A. Kuzmin, and J. Purans, J. Phys.: Condens. Matter **26**, 055401 (2014).
[4] J. Timoshenko, K. R. Keller, and A. I. Frenkel, J. Chem. Phys. **146**, 114201 (2017).
[5] J. Timoshenko and A. I. Frenkel, Catal. Today **280**, 274 (2017).
[6] A. Sutton and J. Chen, Phil. Mag. Lett. **61**, 139 (1990).
[7] X. Dai, Y. Kong, J. Li, and B. Liu, J. Phys: Condens. Matter **18**, 4527 (2006).
[8] J. D. Gale, Phil. Mag. B **73**, 3 (1996).
[9] J. D. Gale and A. L. Rohl, Mol. Simul. **29**, 291 (2003).
[10] Z. Basinski, W. Hume-Rothery, and A. Sutton, in *Proceedings of the Royal Society of London A: Mathematical, Physical and Engineering Sciences* (The Royal Society, 1955), vol. 229, pp. 459–467.
[11] S. Kim, C. Petersen, F. Jona, and P. Marcus, Phys. Rev. B **54**, 2184 (1996).
[12] X. Ou, Mater. Sci. Technol. **33**, 822 (2017).
[13] W. G. Hoover, Phys. Rev. A **31**, 1695 (1985).
[14] R. W. Hockney, Methods Comput. Phys. **9**, 136 (1970).
[15] A. Ankudinov, B. Ravel, J. Rehr, and S. Conradson, Phys. Rev. B **58**, 7565 (1998).
[16] A. I. Frenkel, O. Kleifeld, S. R. Wasserman, and I. Sagi, J. Chem. Phys. **116**, 9449 (2002).
[17] J. A. Varnell, C. Edmund, C. E. Schulz, T. T. Fister, R. T. Haasch, J. Timoshenko, A. I. Frenkel, and A. A. Gewirth, Nat. Commun. **7**, 12582 (2016).